Precise Fault Location in Distribution Networks Based on Optimal Monitor Allocation

Haotian Sun, Hao Yi, *Member, IEEE*, Fang Zhuo, *Member, IEEE*, Xiaotong Du, and Guangyu Yang

***Abstract*—This article presents a novel fault-location method for unbalanced distribution networks in the presence of distributed generations. By utilizing the linear least square method, the candidate faulty lines are selected, and the injected fault currents are derived from the sparse voltage phasor measurements. According to the obtainability of the fault currents, two types of approaches are adopted for estimating the per-unit fault location. By taking advantage of the precise fault-location scheme, the actual faulted line and the accurate fault location are identified. Also, in order to compromise between the fault-location accuracy and the allocation costs, an optimal monitor-allocation algorithm is developed for determining the Pareto-optimal set of meter placements that have the minimal number of monitors to satisfy the requirements of fault-location accuracy. The proposed optimal allocation algorithm and the two types of fault-location approaches are validated on a modified IEEE 123-node test feeder using Matlab and Simulink.**

***Index Terms*—Fault location, distribution networks, distributed generations, linear least square method, cosine similarity, nonlinear optimization, multi-objective optimization.**

I. Introduction

PRECISE fault location (FL) in distribution networks facilitates power restoration and network reconfiguration for lowering outage time, reducing operation costs and thus enhancing the system reliability and power quality indices [1].

In distribution networks, the traditional FL methods that are developed for the transmission systems cannot be applied straightforwardly, due to the presence of non-homogenous lines, the unbalanced loads, as well as the various branches and laterals. Moreover, the increasing penetration of the distributed generations (DGs) poses more challenges to the FL issue. The DG fault-current contributions are usually dependent on various DG characteristics such as DG type, short-circuit capacity, installation position, and somehow low voltage ride through capacity [2], [3]. It is strenuous to incorporate with the various during-fault behaviors of each DG unit [4]. Therefore, it is significant to develop an FL method that is efficient in distribution networks and immune to the impact of DGs.

With the awareness of the aforementioned issues, diverse FL methods are proposed in the literature for the distribution networks. These methods can be categorized into three main families: 1) methods utilizing voltage and current measurements; 2) methods based on high-frequency transients; 3) methods harnessing big data and machine learning techniques.

The voltages and currents information measured across the system are involved in the first group of methods. In [5], the voltage and the current captured at the local substation are utilized to solve complex power equations for the FL. By equally utilizing the substation voltage and current with the addition of the voltage phasors at DG units, reference [6] estimates the FL in an iterative voltage matching procedure. Authors of [7] take advantage of the compressive sensing technique to identify the faulty bus with only voltage phasors monitored at several buses. The graph-based approaches are explored in [8] and [9]. In [8], the fault section is determined by using the network partitioning. Based on the information provided by the downstream fault indicators, reference [9] performs graph marking techniques for estimating the FL. As suggested in [10], ground faults are located iteratively, based on the voltages measured at the MV/LV transformers. The approach in [11] utilizes a new formation of impedance matrix to select the faulty lines via both linear or non-linear least square techniques.

The high-frequency transients based methods formulate the FL by the propagation time of the traveling waves such as electromechanical-waves [12], and reclosure-generating waves [13]. Besides, an approach based on high-frequency fault information is suggested in [14] to cancel the impacts of DG control loops. These schemes can generate highly accurate FL results. However, high-speed synchronizations are also indispensable, which makes these methods less attractive.

The emerging big data concepts and the machine learning techniques are also adopted in the FL issues. In [15]–[17], concepts such as data mining, cloud computing, and data clustering are explored for determining the FL. These methods usually show good adaptivity in different distribution networks but may suffer from the communication issue of the distributed devices and high computational costs.

In the aforementioned literature reviews, the voltage measurements are generally required for precise FL estimation. Some of these methods also need current measurements. However, the current measurements are affected by the saturation of the

Manuscript received April 9, 2019; revised July 21, 2019 and September 25, 2019; accepted November 16, 2019. Date of publication November 19, 2019; date of current version July 23, 2020. This work was supported in part by the National Natural Science Foundation of China under Grant 51977172, in part by the Science and Technology Project of State Grid Corporation of China under Grant 52110418000S, and in part by the Open Fund of Jiangsu Engineering Technology Research Center for Energy Storage Conversion and Application under Grant NYN51201901280. Paper no. TPWRD-00391-2019. *(Corresponding author: Hao Yi.)*

The authors are with the State Key Laboratory of Electrical Insulation and Power Equipment, Xi'an Jiaotong University, Xi'an 710049, China (e-mail: sunhaotian@stu.xjtu.edu.cn; yi_hao@xjtu.edu.cn; zffz@mail.xjtu.edu.cn; doxato@stu.xjtu.edu.cn; yangguangyu@stu.xjtu.edu.cn).

Color versions of one or more of the figures in this article are available online at http://ieeexplore.ieee.org.

Digital Object Identifier 10.1109/TPWRD.2019.2954460

current transformers. The degradation in current measurement accuracy deteriorates the FL estimation errors. Consequently, an FL method utilizing only voltage measurements is highly required.

Moreover, in order to accurately pinpoint the fault location, an adequate number of measurement units are entailed at several buses. However, this may yield considerable cost for monitor allocation. Therefore, it necessitates an optimal monitor allocation algorithm that can compromise between the competitive objectives such as FL accuracy and allocation costs, so as to minimize the number of monitors needed for the expected accuracy level.

To achieve the above-mentioned functionalities, this paper introduces a novel FL method as well as an optimal monitor allocation algorithm for distribution networks in the presence of DG units. Instead of involving the measured currents data, the proposed FL scheme only utilizes voltage phasor measurements at a few buses that are efficiently determined by the proposed monitor-allocation optimization algorithm. It is assumed that the system topology, as well as the impedance information, are available and that the DGs are distributed at nonadjacent buses. Besides, it is assumed that the pre-fault and during-fault voltage phasors are measured synchronously at the monitor-equipped buses.

The rest of this paper is organized as follows. Section II illustrates a general fault analysis in distribution networks with DGs. Section III describes the methodology of the proposed FL algorithm. Section IV formulates the monitor allocation problem and develops the optimization strategy. Case studies based on the simulation results are reported in Section V. Section VI represents the conclusion.

II. Fault Analysis on Distribution Systems in Presence of DGs

In the proposed method, the unbalanced laterals and the capacitive parameters of distribution lines are considered by utilizing an equivalent π model [18]. Note that for two-phase or single-phase line, elements of non-existing phases are set to zero and added so that each matrix is of size 3×3.

Suppose that the examined system has N buses and L lines. In the system, M buses are monitored, and S buses are connected with DGs. The DG-connected buses are numbered from dg-*1* to dg-S. Without losing generality, a fault of any type is assumed to occur at the point F along the line i-j. The per-unit fault distance from bus i is denoted m. The during-fault voltage vector at the fault point is denoted $[U_F]$. Then the fault current injected at node F can be expressed [19]:

$$[I_f] = -Y_f \cdot [K_f] \cdot [U_F] \tag{1}$$

where Y_f stands for the fault admittance coefficient; the fault matrix $[K_f]$ is independent of Y_f, and its determination only requires the knowledge of the fault type [1].

Considering the impact of monitor allocation, the impedance matrix is modified by eliminating rows that correspond to unmonitored buses. Note that in this paper, the undermentioned impedance matrix always refers to the modified one.

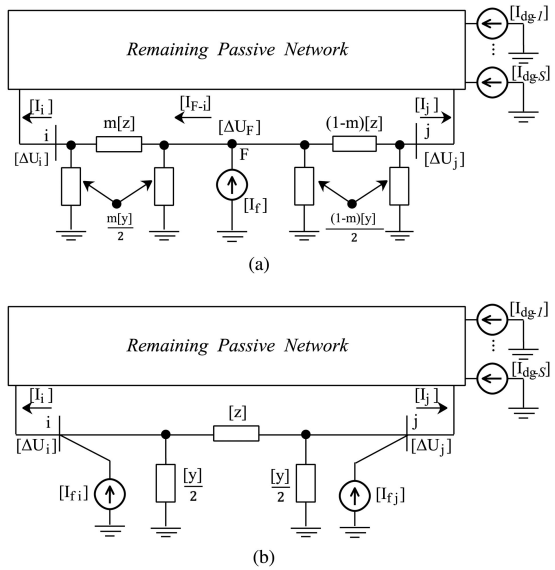

Fig. 1. Single-line representation of faulted system equivalence. (a) before equivalencing I_f. (b) after equivalencing I_f into I_{fi}, I_{fj}.

Let P_n denote the number of existing phases at the n-th bus. The number of phases along the line i-j is determined:

$$P_{i\text{-}j} = \min(P_i, P_j) \tag{2}$$

To account for the impact of the DGs, three types of DGs are mainly considered in this paper:

1) the conventional rotating generators that are directly coupled to the system. During fault conditions, these DGs can be represented by the Thevenin equivalent models [3];
2) the doubly-fed asynchronous generators (DFIG) that usually have the crowbar scheme and behave like the first type DGs [20];
3) the converter interfaced DGs that have contributions to the steady-state fault current [3].

In the following discussions, these DGs are assumed to have the capability to ride through faults. The steady-state fault current contributions of these DGs are treated as the current injections at the connection buses [2], [3]. Therefore, the DGs' parameters and characteristics are not required to be known, and the internal impedance of these DGs are not included in the impedance matrix. This idea prevents the modeling errors of the DGs' internal behaviors and is not affected by the various control schemes or the complex features of the DGs [6].

From the aforementioned analysis, the fault current injections in the fault-superimposed network are contributed by two parts: 1) fault current that is injected at fault point F; 2) DG currents that are injected at DG-connected buses. These two components are analyzed separately.

As depicted in Fig. 1, without any change of the remaining network, the fault current $[I_f]$ can be equivalent to two current sources $[I_{fi}]$, $[I_{fj}]$ that are injected at bus i and j[11]. Therefore, by utilizing some columns in the bus impedance matrix, the voltage drops $[\Delta U_{rec}]$ that are recorded by the monitors can be

represented as follows:

$$[\Delta U_{\text{rec}}] = [Z_i] \cdot [I_{\text{fi}}] + [Z_j] \cdot [I_{\text{fj}}] + \sum_{n=1}^{S} [Z_{\text{dg-}n}] \cdot [I_{\text{dg-}n}] \quad (3)$$

where $[Z_n]$ denotes the column vectors in the impedance matrix corresponding to the faulty phases of the n-th bus; $[I_{\text{dg-}n}]$ is the DG-injection current vector at bus n. Note that each of $[Z_i]$ and $[Z_j]$ has $P_{\text{i-j}}$ columns.

Using Kirchhoff's voltage and current laws, some relations between the quantities in Fig. 1 are derived as follows:

- In the line segment $i - F$ of Fig. 1a:

$$\begin{bmatrix} [\Delta U_F^{(\text{fp})}] \\ [I_{F-i}^{(\text{fp})}] \end{bmatrix} = \begin{bmatrix} [A(m)] & [B(m)] \\ [C(m)] & [D(m)] \end{bmatrix} \cdot \begin{bmatrix} [\Delta U_i^{(\text{fp})}] \\ [I_i^{(\text{fp})}] \end{bmatrix} \quad (4)$$

$$\begin{bmatrix} [\Delta U_F^{(\text{dg})}] \\ [I_{F-i}^{(\text{dg})}] \end{bmatrix} = \begin{bmatrix} [A(m)] & [B(m)] \\ [C(m)] & [D(m)] \end{bmatrix} \cdot \begin{bmatrix} [\Delta U_i^{(\text{dg})}] \\ [I_i^{(\text{dg})}] \end{bmatrix} \quad (5)$$

- In the line segment $F - j$ of Fig. 1a:

$$\begin{bmatrix} [\Delta U_F^{(\text{fp})}] \\ [I_f] - [I_{F-i}^{(\text{fp})}] \end{bmatrix} = \begin{bmatrix} [A(m')] & [B(m')] \\ [C(m')] & [D(m')] \end{bmatrix} \cdot \begin{bmatrix} [\Delta U_j^{(\text{fp})}] \\ [I_j^{(\text{fp})}] \end{bmatrix} \quad (6)$$

$$\begin{bmatrix} [\Delta U_F^{(\text{dg})}] \\ -[I_{F-i}^{(\text{dg})}] \end{bmatrix} = \begin{bmatrix} [A(m')] & [B(m')] \\ [C(m')] & [D(m')] \end{bmatrix} \cdot \begin{bmatrix} [\Delta U_j^{(\text{dg})}] \\ [I_j^{(\text{dg})}] \end{bmatrix} \quad (7)$$

- In the line segment $i - j$ of Fig. 1b:

$$\begin{bmatrix} [\Delta U_i^{(\text{fp})}] \\ [I_{\text{fi}}] - [I_i^{(\text{fp})}] \end{bmatrix} = \begin{bmatrix} [A(1)] & [B(1)] \\ [C(1)] & [D(1)] \end{bmatrix} \cdot \begin{bmatrix} [\Delta U_j^{(\text{fp})}] \\ [I_j^{(\text{fp})}] - [I_{\text{fj}}] \end{bmatrix} \quad (8)$$

- By definition of the bus impedance matrix:

$$\begin{bmatrix} [\Delta U_i^{(\text{fp})}] \\ [\Delta U_j^{(\text{fp})}] \end{bmatrix} = \begin{bmatrix} [Z_{ii}] & [Z_{ij}] \\ [Z_{ij}] & [Z_{jj}] \end{bmatrix} \cdot \begin{bmatrix} [I_{\text{fi}}] \\ [I_{\text{fj}}] \end{bmatrix} \quad (9)$$

$$\begin{bmatrix} [\Delta U_i^{(\text{dg})}] \\ [\Delta U_j^{(\text{dg})}] \end{bmatrix} = \begin{bmatrix} [Z_{i,\text{dg-1}}] & \dots & [Z_{i,\text{dg-}S}] \\ [Z_{j,\text{dg-1}}] & \dots & [Z_{j,\text{dg-}S}] \end{bmatrix} \cdot \begin{bmatrix} I_{\text{dg}} \end{bmatrix} \quad (10)$$

where A, B, C and D are the line parameters expressed in Appendix A; m' is the complement per-unit FL: $m' = 1 - m$; the superscripts (fp) and (dg) represent the superimposed components yielded by the fault current $[I_f]$ and the DG-injection currents $[I_{\text{dg-}n}]$, respectively; $[I_{\text{dg}}]$ denotes the column vector $[[I_{\text{dg-1}}]^T \dots [I_{\text{dg-}S}]^T]^T$; and $[Z_{nr}]$ stands for the transfer impedance matrix between bus n and bus r that is derived from the original impedance matrix.

As detailed in Appendix A, the relations between $[I_{\text{fi}}]$, $[I_{\text{fj}}]$ and $[U_F]$ can be derived from (4)–(10) as follows:

$$[I_{\text{fi}}] = [T_1] \cdot [I_f] \quad (11)$$

$$[I_{\text{fj}}] = [T_2] \cdot [I_f] \quad (12)$$

$$[U_F] = [U_F^{(\text{pre})}] + [T_3] \cdot [I_f] + \sum_{n=1}^{S} ([W_1] \cdot [Z_{i,\text{dg-}n}] + [W_2] \cdot [Z_{j,\text{dg-}n}]) \cdot [I_{\text{dg-}n}] \quad (13)$$

where $[T_1]$, $[T_2]$, $[T_3]$, $[W_1]$ and $[W_2]$ are coefficients in function of fault position m and the network parameters. $[U_F^{(\text{pre})}]$ indicates the pre-fault voltage at F.

If the pre-fault voltages $[U_i^{(\text{pre})}]$ and $[U_j^{(\text{pre})}]$ are known, $[U_F^{(\text{pre})}]$ can be expressed in (14). If not, $[U_F^{(\text{pre})}]$ is simply assumed as 1.0 p.u.

$$[U_F^{(\text{pre})}] = [W_1] \cdot [U_i^{(\text{pre})}] + [W_2] \cdot [U_j^{(\text{pre})}] \quad (14)$$

III. Fault-Location Methodology

Generally, in the proposed FL method, the fault is located in three steps: 1) the derivation of the fault currents, 2) the faulted-line candidate selection, and 3) the precise FL estimation and the identification of the real FL.

A. Derivation of Fault Currents

Let $\mathbf{Z_{total}}$ denote the set $\{[Z_i], [Z_j], [Z_{\text{dg-1}}], \dots, [Z_{\text{dg-}S}]\}$ and $\mathbf{Z_{dg}}$ represent $\{[Z_{\text{dg-1}}], \dots, [Z_{\text{dg-}S}]\}$. Suppose that the rank of the set $\mathbf{Z_{dg}}$ is designated by r_{dg}, and the set of $\mathbf{Z_{total}}$ has rank r_{total}. Define the rank difference $\Delta r = r_{\text{total}} - r_{\text{dg}}$.

In the proposed FL method, two assumptions are made:

- *Assumption 1:* the impedance column vectors corresponding to the DG-equipped buses are linearly independent;
- *Assumption 2:* the rank Δr satisfies $\Delta r \geq P_{i\text{-}j}$.

These two assumptions are achieved by the optimal monitor allocation that will be introduced in Section IV.

Due to the sparse allocation of measurement units, the set of impedance column vectors involved in (3) are not always linearly independent. As a result, the values of some phases in $[I_{\text{fi}}]$, $[I_{\text{fj}}]$ are mixed and thus not obtainable.

Let us rewrite $\mathbf{Z_{total}}$ by phase as $\{[Z_{i\text{-}j}^{(1)}], \dots, [Z_{i\text{-}j}^{(2\cdot P_{\text{i-j}})}], [Z_{\text{dg}}^{(1)}], \dots, [Z_{\text{dg}}^{(r_{\text{dg}})}]\}$. Then the maximal linearly independent set (MLIS) of $\mathbf{Z_{total}}$ is expressed in (15).

$$[Z_{\text{MLIS}}] = \left[[Z_{i\text{-}j}^{(1)}], \dots, [Z_{i\text{-}j}^{(\Delta r)}], [Z_{\text{dg}}^{(1)}], \dots, [Z_{\text{dg}}^{(r_{\text{dg}})}]\right] \quad (15)$$

where $[Z_{i\text{-}j}^{(1)}], \dots, [Z_{i\text{-}j}^{(\Delta r)}]$ stand for the impedance vectors of the MLIS-selected phases at bus i, j. Note that $\mathbf{Z_{dg}}$ is fully included in $[Z_{\text{MLIS}}]$ because of Assumption 1.

The MLIS can be regarded as a set of basis to express the set of vectors $\{[Z_{i\text{-}j}^{(1)}], \dots, [Z_{i\text{-}j}^{(2\cdot P_{\text{i-j}})}]\}$:

$$[Z_{i\text{-}j}^{(n)}] = \sum_{u=1}^{\Delta r} k_u^{(n)} \cdot [Z_{i\text{-}j}^{(u)}] + \sum_{v=1}^{r_{\text{dg}}} p_v^{(n)} \cdot [Z_{\text{dg}}^{(v)}] \quad (16)$$

where the coefficients $k_u^{(n)}$ and $p_v^{(n)}$ can be obtained by applying the Gauss-Jordan elimination to the set $\mathbf{Z_{total}}$.

Substituting (16) into (3):

$$[\Delta U_{\text{rec}}] = [Z_{\text{MLIS}}] \cdot [I_{\text{eq}}] \quad (17)$$

with $[I_{\text{eq}}]$ expressed in (18):

$$\begin{bmatrix}[I_{\text{eq}}^{(i\text{-}j)}]\\ [I_{\text{eq}}^{(\text{dg})}]\end{bmatrix} = \begin{bmatrix}[k_{(i)}] & [k_{(j)}] & [O]\\ [p_{(i)}] & [p_{(j)}] & [I]\end{bmatrix} \cdot \begin{bmatrix}[I_{\text{f}i}]\\ [I_{\text{f}j}]\\ [I_{\text{dg}}]\end{bmatrix} \tag{18}$$

where the specific expressions of $[k_{(i)}], [k_{(j)}], [p_{(i)}], [p_{(j)}]$ are given in (19); $[O]$ and $[I]$ indicates the zero matrix (of size $\Delta r \times \Delta r$) and the identity matrix (of size $r_{\text{dg}} \times r_{\text{dg}}$), respectively.

$$\begin{bmatrix}[k_{(i)}][k_{(j)}]\\ [p_{(i)}][p_{(j)}]\end{bmatrix} = \left[\begin{array}{ccc|ccc} k_1^{(1)} & \cdots & k_1^{(P_{\text{i-j}})} & k_1^{(P_{\text{i-j}}+1)} & \cdots & k_1^{(2\cdot P_{\text{i-j}})}\\ \vdots & & & \vdots & & \\ k_{\Delta r}^{(1)} & \cdots & k_{\Delta r}^{(P_{\text{i-j}})} & k_{\Delta r}^{(P_{\text{i-j}}+1)} & \cdots & k_{\Delta r}^{(2\cdot P_{\text{i-j}})}\\ \hline p_1^{(1)} & \cdots & p_1^{(P_{\text{i-j}})} & p_1^{(P_{\text{i-j}}+1)} & \cdots & p_1^{(2\cdot P_{\text{i-j}})}\\ \vdots & & & \vdots & & \\ p_{r_{\text{dg}}}^{(1)} & \cdots & p_{r_{\text{dg}}}^{(P_{\text{i-j}})} & p_{r_{\text{dg}}}^{(P_{\text{i-j}}+1)} & \cdots & p_{r_{\text{dg}}}^{(2\cdot P_{\text{i-j}})} \end{array}\right] \tag{19}$$

Then the linear least square (LLS) method for complex domain is adopted to derive the equivalent current vector [21]:

$$[I_{\text{eq}}^*] = (\overline{[Z_{\text{MLIS}}]}^T \cdot [Z_{\text{MLIS}}])^{-1} \cdot \overline{[Z_{\text{MLIS}}]}^T \cdot [\Delta U_{rec}] \tag{20}$$

with the residual error defined as follows:

$$E_{\text{residual}} = ||[\Delta U_{\text{rec}}] - [Z_{\text{MLIS}}] \cdot [I_{\text{eq}}^*]^T|| \tag{21}$$

B. Faulted-Line Candidate Selection

Based on the discussion above, faulted-line candidate selection can be performed. For each line l in the examined system, the corresponding $[Z_{\text{MLIS}}^{(l)}]$ is generated by utilizing (15). Then the equivalent current vector $[I_{\text{eq}}^{(l)}]$ and the residual error $E_{\text{residual}}^{(l)}$ can be obtained by applying (20) and (21), respectively. The criterion to distinguish the candidate faulty lines is described as follows:

- *Criterion 1:* the candidate faulty lines l should satisfy:

$$E_{\text{residual}}^{(l)} < \delta_E \tag{22}$$

where δ_E is the predefined error tolerance.

Every line in the system is examined by (22), and the qualified lines are marked as the candidate faulty lines. Then two types of precise FL methods are applied to each candidate, depending on the rank difference Δr. From the aforementioned discussion, Δr can be interpreted as the number of obtainable phases of $[I_{\text{f}i}]$ and $[I_{\text{f}j}]$. It is also evinced that each of $[I_f]$, $[I_{\text{f}i}]$ and $[I_{\text{f}j}]$ has $P_{\text{i-j}}$ phases.

C. Precise FL Method for Complete Case (Type-I Method)

In the complete case where $\Delta r = 2 \cdot P_{\text{i-j}}$, each phase of $[I_{\text{f}i}], [I_{\text{f}j}]$ can be obtained from $[I_{\text{eq}}^*]$.

By substituting the values of $[I_{\text{f}i}], [I_{\text{f}j}]$ in (11) (12) and eliminating $[I_f]$:

$$[a_2] \cdot m^2 + [a_1] \cdot m + [a_0] = 0 \tag{23}$$

where $[a_2], [a_1], [a_0]$ are the 3×1 coefficient vectors determined by the line impedance parameters and the obtained currents $[I_{\text{f}i}], [I_{\text{f}j}]$. Their expressions are given in detail in Appendix B.

In the case where the examined line contains only a single phase, (23) is a simple quadratic equation with two complex solutions; in the other cases where the examined line has two or three phases, (23) is a set of overdetermined quadratic equations. Due to the residual error of the LLS, the general solutions to these overdetermined equations may not exist. Therefore, each of these quadratic equations is solved separately for two complex solutions. The criterion to distinguish real solutions is expressed as follows:

- *Criterion 2:* in all complex solutions to (23), the real solutions m^* should satisfy:

$$\left|\left|\frac{\text{Im}(m^*)}{\text{Re}(m^*)}\right|\right| < \delta_m \text{ and } ||m^*|| \in [0, 1] \tag{24}$$

where δ_m is the predefined tolerance of the imaginary component.

By applying (24) to all complex solutions, the real parts of the qualified solutions are extracted and marked as the estimated FL for the examined candidate line. Note that this type of method is independent of fault type and fault impedance.

D. Precise FL Method for Degraded Case (Type-II Method)

The type-II method assumes the fault type to be known, such that $[K_f]$ in (1) can be determined. This method also assumes that the fault impedance is resistive, i.e., $Y_f \in R$.

In the degraded case where $\Delta r < 2 \cdot P_{\text{i-j}}$, $[I_{\text{f}i}]$ and $[I_{\text{f}j}]$ are mixed in $[I_{\text{eq}}^*]$ and cannot be fully derived.

By substituting (11), (12) into (18):

$$[I_{\text{eq}}^{(i\text{-}j)}] = ([k_{(i)}] \cdot [T_1] + [k_{(j)}] \cdot [T_2]) \cdot [I_f] \tag{25}$$

$$[I_{\text{dg-}n}] = [I_{\text{eq}}^{(\text{dg})}] - ([p_{(i)}] \cdot [T_1] + [p_{(j)}] \cdot [T_2]) \cdot [I_f] \tag{26}$$

According to the aforementioned Assumption 2, equation (25) is overdetermined or properly determined. Therefore for a given m, $[I_f]$ can be solved by substituting (20) into (25). Then $[I_{\text{dg-}n}]$ can be obtained by (26).

By combining (1), (3), (11)–(13) and rearranging:

$$[U_{\text{left}}] = Y_f \cdot [U_{\text{right}}] \tag{27}$$

where

$$[U_{\text{left}}] = [\Delta U_{\text{rec}}] - \sum_{n=1}^{S} [Z_{\text{dg-}n}] \cdot [I_{\text{dg-}n}] \tag{28}$$

$$[U_{\text{right}}] = -([Z_i] \cdot [T_1] + [Z_j] \cdot [T_2]) \cdot [K_f] \cdot [U_F] \tag{29}$$

Since Y_f is a real number, $[U_{\text{left}}]$ and $[U_{\text{right}}]$ in (27) will be parallel, if the actual value of m is adopted. To quantize the orientation similarity of the two vectors, we harness the centered cosine similarity (CCS) that measures the cosine angle between the two vectors, as in (30). The larger value of the CCS reveals the more similar orientation of the vectors.

$$\text{CosSim}(x, \mu) = \frac{\langle x - \bar{x}, \mu - \bar{\mu} \rangle}{||x - \bar{x}|| \cdot ||\mu - \bar{\mu}||} \tag{30}$$

where $\langle , \rangle$ is the inner-product operator.

Therefore, the actual FL can be solved by locating the maximum value of the CCS between $[U_{\text{left}}]$ and $[U_{\text{right}}]$. Since the CCS only applies in the real domain, the real and imaginary parts of $[U_{\text{left}}]$ and $[U_{\text{right}}]$ are separated and reshaped. Note that the maximization of $\text{CosSim}((x,\mu))$ is equivalent to the minimization of the function $(\text{CosSim}((x,\mu))+1)^{-1}$.

The constrained minimization problem of variable m is formed as follows:

$$\min_{m\in[0,1]} \left(\text{CosSim} \left(\begin{bmatrix} \text{Re}([U_{\text{left}}]) \\ \text{Im}([U_{\text{left}}]) \end{bmatrix}, \begin{bmatrix} \text{Re}([U_{\text{right}}]) \\ \text{Im}([U_{\text{right}}]) \end{bmatrix} \right) + 1 \right)^{-1} \tag{31}$$

By substituting a surrogate variable m_s as in (32), the bound constrained problem (31) can be transformed into an unconstrained non-linear optimization problem and thus can be solved by the Nelder-Mead simplex algorithm [22], [23]. This algorithm utilizes a two-point simplex and modifies the simplex iteratively to search m_s that minimizes (31). After that m_s is obtained, m can be simply derived from (32).

$$m = 0.5 \cdot (\sin(m_s) + 1) \tag{32}$$

After obtaining the candidate FL solutions with the type-I and II method, further identification for the truly faulty line as well as the real FL is carried out. For each candidate line, the function in (31) is calculated by the estimated FL m. Finally, the line with the minimum value of the CCS in (31) is selected as the faulty line, and the corresponding m is chosen as the precise fault location. The complete procedure of the proposed FL method is depicted in Fig. 2.

IV. Optimal Monitor-Allocation Algorithm

Generally, the proposed monitor-allocation algorithm optimizes at two aspects: 1) the minimization of allocation cost and 2) the maximization of the FL accuracy.

Regarding the relation between Δr and the two cases discussed above, two conditions can be deduced:

- *Condition 1:* to achieve the complete case where both $[I_{\text{f}i}]$ and $[I_{\text{f}j}]$ are derivable from (18), Δr must satisfy:

$$\Delta r = 2 \cdot P_{\text{i-j}} \tag{33}$$

- *Condition 2:* in the degraded case, to make $[I_f]$ derivable, Δr must satisfy:

$$\Delta r \geq P_{\text{i-j}} \tag{34}$$

Note that for all lines in the examined system, the lines satisfying the condition 1 are in the complete case where the aforementioned type-I method can be applied, whereas the rest of lines are in the degraded case where the type-II method should be adopted.

Let us define the binary decision vector $x \in \{0,1\}^N$ whose n-th element x_n equals 1 if bus n is equipped with a monitor and equals 0 if bus n is not monitored. For each combination of the decision vector, the corresponding modified impedance matrix is extracted. Also, for the l-th line, define a binary indicator $q_l^{(t)}$ whose value equals 1 if the condition t is satisfied

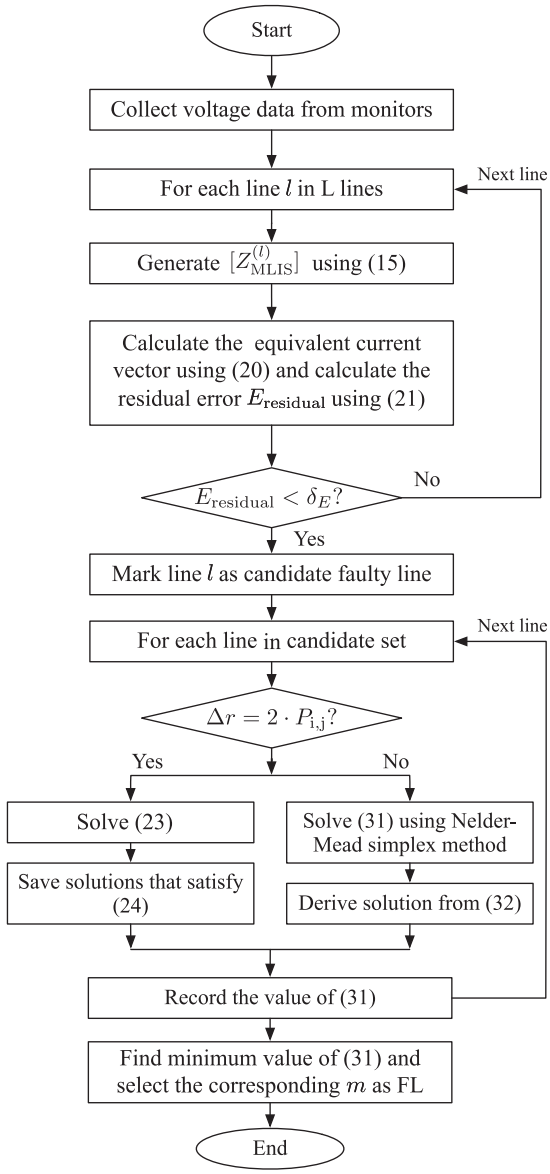

Fig. 2. Flowchart of the proposed FL method.

or otherwise equals 0. Then the multi-objective optimization problem (MOOP) can be formed in the decision space $\{0,1\}^N$.

- Objective function 1: to minimize the total cost [24]:

$$\min_{x\in\{0,1\}^N} \sum_{n=1}^{N} c_n \cdot x_n \tag{35}$$

where c_n stands for the monitor installation and maintenance cost at bus n.

- Objective function 2: the total accuracy level can be enhanced if fewer lines are in the degraded case. Therefore, the number of lines that do not satisfy the condition 2 should be minimized. Recall that L represents the number of lines in the examined system. This objective can be expressed

as follows:

$$\min_{x\in\{0,1\}^N}\left(L-\sum_{l=1}^{L}q_l^{(1)}\right) \tag{36}$$

In addition, two constraints are made such that the two assumptions that are made in Section III can be satisfied.

- Constraint function 1: to validate the Assumption 1, the set $\mathbf{Z_{dg}}$ must have full column rank, i.e.

$$r_{\text{dg}}-\sum_{n=1}^{S}P_{\text{dg-}n}=0 \tag{37}$$

- Constraint function 2: to validate the Assumption 2, the condition 2 must be satisfied for every line, i.e.

$$\sum_{l=1}^{L}q_l^{(2)}-L=0 \tag{38}$$

It is noted that deploying more monitors in the system reduces the number of lines in the degraded cases and consequently leads to more accurate FL estimations. However, an increasing number of monitors also yields higher expenses for device installation and maintenance. Therefore, the two objectives in (35) and (36) are competitive. This implies that the globally optimal solution that generates both minimal cost and maximal FL accuracy does not exist. The trade-off between the conflicting objectives can be found in the Pareto-optimal solutions. For each Pareto-optimal solution, there do not exist other solutions that have better performance for both objectives at the same time [25]. These solutions can provide guidance to compromise between the accuracy and the cost. For an expected level of the FL accuracy, the best solution can be found on the Pareto front, which satisfies the accuracy requirement with the minimal number of monitors. On the other hand, if the budget of monitor allocation, rather than the accuracy requirement, is determined, the optimal solution can also be established which yields the highest FL accuracy within the budget. Therefore, the Pareto-optimality helps to determine the monitor planning with good flexibility to different scenarios.

To obtain the Pareto-optimums, the non-dominated sorting genetic algorithm-II (NSGA-II) can be adopted [26]. The NSGA-II applies the non-dominated sorting in the combination of parents and children population. The generations are iteratively produced by genetic operators, while the chromosomes are repetitively selected based on diversity. After a sufficient number of iterations, when each solution cannot be further improved regarding one objective without degrading the other, the NSGA-II program is said to reach convergence, and the Pareto-optimality is obtained.

V. Case Studies

To validate the proposed FL method, the modified IEEE 123 node test feeder model, shown in Fig. 3, is simulated by Mathworks Simulink. The test feeder contains the single, double and three-phase laterals and sublaterals, unbalanced spot loads, and shunt capacitor banks, and has been commonly used in the literature concerning the fault location issues.

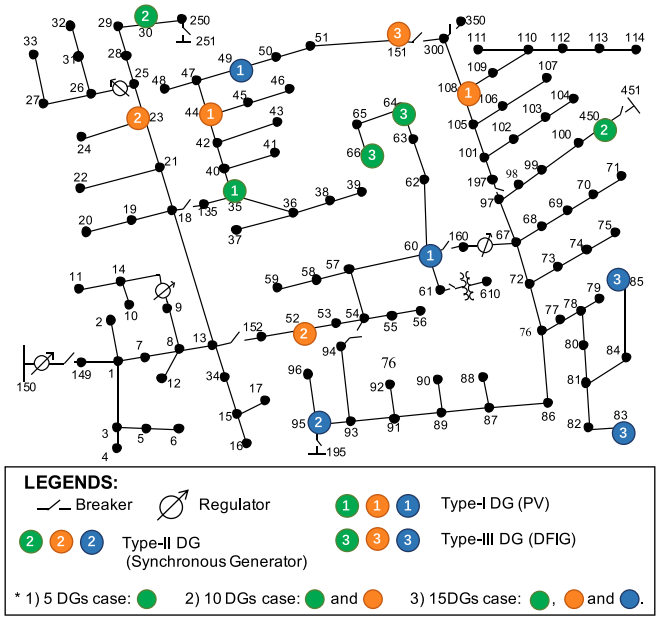

Fig. 3. Single-line diagram of the simulated 123-node distribution system connected with three types of DGs allocated in three cases.

As a result of the modification, the spot loads are modeled as constant impedances, and the voltage regulators are removed for simplification, whereas three types of DGs, including inverter-based PV, synchronous generators and double-fed induction generators (DFIG), are arbitrarily connected into the test feeder in four cases: 1) 0 DGs 2) 5 DGs 3) 10 DGs 4) 15 DGs. All fault types including LG (single-phase-to-ground faults), LL (phase-to-phase faults), LLG (double-phase-to-ground faults), and LLLG (three-phase-to-ground faults) are simulated at 10%, 30%, 50%, 70%, and 90% of each line, with 0.1 Ω, 20 Ω, 50 Ω and 100 Ω fault resistances and in presence of 0, 5, 10 and 15 DGs. For each test case, the pre-fault and during-fault synchronized voltage phasors are measured at each monitored bus. The additional zero-mean complex Gaussian noises with standard deviation σ are generated to test the performance of the proposed method with errors in voltage measurements, synchronization, and line impedance data. The impact of sampling rate and different grounding mode are also examined. The proposed FL method is implemented and tested on Matlab. The percentage error $E_{\%}$ of FL estimation is defined as follows [27]:

$$E_{\%}=|m_e-m_t|\times 100\% \tag{39}$$

where m_e stands for the estimated per-unit FL; m_t is the true per-unit FL.

A. Implementation of Monitor Allocation Algorithm

Before the accuracy test of the proposed FL method, the optimal monitor allocation problems for 5, 10 and 15-DG allocations are solved separately by the NSGA-II, as described in Section IV. The cost for each bus is assumed to equal. The NSGA-II is programmed on Matlab and initialized with 150 populations. The iteration number is limited up to 500. After

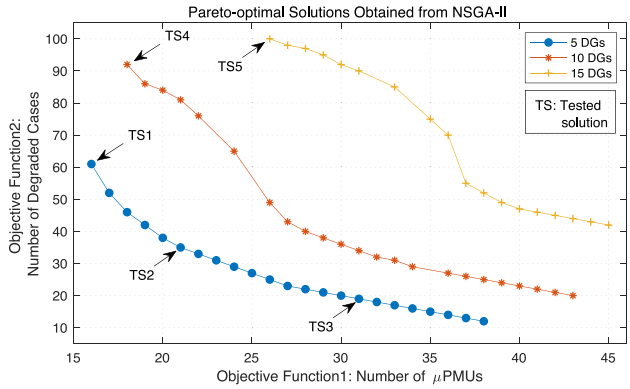

Fig. 4. Pareto-optimal results using NSGA-II for two objective functions.

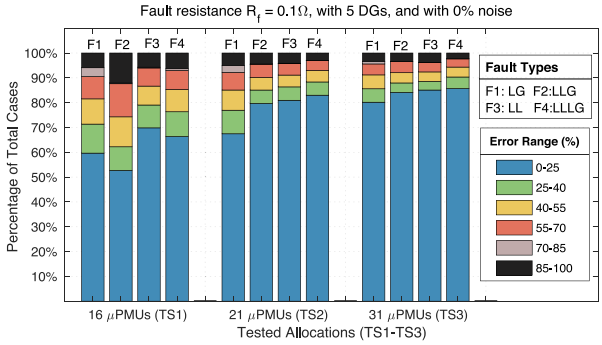

Fig. 5. Stacked histogram representing the percentage error distributions of FL estimation under three μPMU allocations.

around 300 iterations, the intermediate solutions for all three optimization problems achieve convergence. When the program reaches the maximum iterations, the final results of the NSGA-II program are obtained as the Pareto-optimal solutions, as shown in Fig. 4.

To illustrate the trade-off between the FL accuracy and the cost, five Pareto-optimal solutions are selected and tested:

- Tested solution 1 (for 0 and 5 DGs): 16 μPMUs are allocated at bus 11, 22, 37, 39, 42, 56, 57, 65, 66, 83, 98, 100, 114, 151, 250 and 450;
- Tested solution 2 (for 5 DGs): 21 μPMUs are allocated at bus 11, 22, 29, 37, 39, 42, 56, 57, 65, 66, 71, 83, 95, 98, 100, 114, 150, 151, 250, 300 and 450;
- Tested solution 3 (for 5 DGs): 31 μPMUs are allocated at bus 6, 11, 16, 22, 27, 29, 32, 37, 39, 42, 46, 56, 57, 59, 63, 65, 66, 71, 75, 83, 95, 98, 100, 104, 111, 114, 150, 151, 250, 300 and 450;
- Tested solution 4 (for 10 DGs): 18 μPMUs are allocated at bus 2, 24, 29, 36, 39, 40, 46, 50, 55, 59, 65, 66, 113, 150, 151, 250, 300 and 450;
- Tested solution 5 (for 15 DGs): 26 μPMUs are allocated at bus 6, 22, 24, 33, 36, 41, 42, 45, 47, 51, 55, 57, 61, 62, 64, 65, 66, 72, 79, 83, 96, 113, 151, 250, 300 and 450.

The FL performance for the first three selected allocations is presented in Fig. 5, which shows the percentage proportion of fault cases estimated within each error range for four fault types and three tested allocations with 5 DGs. As shown, FL errors in each type of fault are improved with the increasing number of monitors. In LG faults (F1), for example, around 60% of the test cases are estimated with errors less than 25% (the bar in blue) under 16-monitor placement (TS1). This proportion is raised to more than 75% by adding 5 extra monitors (TS2), and to around 80% by adding 15 extra (TS3).

Table I shows the average and variance of the FL percentage errors with four different fault resistances with 5 DGs. As presented in Table I, among the cases of the fault resistance, the average and the variance of the FL errors changes slightly for each type of fault, which indicates that in the noise-free cases, the proposed method is not greatly affected by the value of the fault resistance. On the other hand, for the 16-monitor placement (TS1), the average and variance of estimation errors do not exceed 27.33% and 9.09%, respectively, which shows a reliable FL accuracy and stability despite the various fault types and fault resistance values. Also, it can be seen from Table I that the increasing number of allocated monitors also results in the decreasing variance of estimation errors. Therefore, the stability of the proposed method is raised by selecting the Pareto-optimal solutions with more monitors.

On the other hand, while the FL performance can be ameliorated by allocating more monitors, the diminishing marginal utility, however, can be observed in Table I: more increment in the number of allocated monitors leads to the less reduction of the error average and variance and therefore less increment in the performance such as the accuracy and stability. Consequently, it necessitates a prior trade-off between the budget for allocating additional monitors and the expected enhancement of the FL performance. Then the best allocation solution can be extracted from the Pareto-optimal set to according to the accuracy expectations or the allocation budgets.

B. Impacts of Number of DGs

Fig. 6 presents the FL errors of four fault types with 0, 5, 10 and 15 DGs. The 16-monitor placement (TS1) is adopted in the 0 and 5-DG cases, while the 18-monitor placement (TS4) and the 26-monitor placement (TS5) are used for the 10 and the 15-DG cases, respectively. It can be seen from Fig. 6 that, compared with the case where 5 DGs are in service, there are reductions in the FL errors for all types of faults when DGs are out of service. This indicates that the performance of the proposed method rises when fewer DGs are in service. As illustrated in Section III, the fact can be interpreted by the decrease in the degraded cases when more DGs are unavailable. More specifically, fewer column vectors corresponding to the DG connection buses are involved in the LLS algorithm, which reduces the number of linearly dependent cases and thus enhances performance. On the other hand, increasing the number of DGs results in the rising error of FL estimation. However, the maximum error for 15 DGs is 36.51%, which is within the acceptable range.

C. Impacts of Measurement Noise

The measurement accuracy of μPMUs may suffer degradation in the occurrence of measurement noises. In order to simulate

TABLE I
AVERAGE AND VARIANCE OF THE PERCENTAGE ERRORS (%) OF FL ESTIMATION FOR NOISELESS CASES WITH 5 DGS

No. of PMUs	Index	$R_f = 0.1\Omega$				$R_f = 20\Omega$				$R_f = 50\Omega$				$R_f = 100\Omega$			
		LG	LLG	LL	LLLG	LG	LLG	LL	LLLG	LG	LLG	LL	LLLG	LG	LLG	LL	LLLG
16	Avg.	24.71	21.74	22.81	24.09	27.33	23.04	22.50	24.25	26.31	20.21	22.73	20.35	26.14	20.71	24.21	19.07
	Var.	7.95	7.43	9.09	8.62	8.13	8.36	8.60	8.71	7.93	7.64	8.34	8.18	7.81	7.62	8.59	7.28
21	Avg.	18.33	10.02	11.66	11.52	19.01	11.50	11.66	11.65	19.88	11.95	11.47	10.41	18.59	11.69	12.18	10.58
	Var.	6.98	4.53	5.64	5.95	7.31	5.51	5.63	6.04	7.64	5.91	5.55	5.19	6.77	5.78	5.91	5.27
31	Avg.	10.92	7.41	9.48	9.37	11.77	9.17	9.48	9.50	12.70	10.91	10.57	10.09	11.55	8.95	10.07	9.05
	Var.	4.86	3.32	4.80	4.86	5.11	4.61	4.80	4.96	5.16	5.21	4.90	4.73	5.14	4.50	5.17	4.56

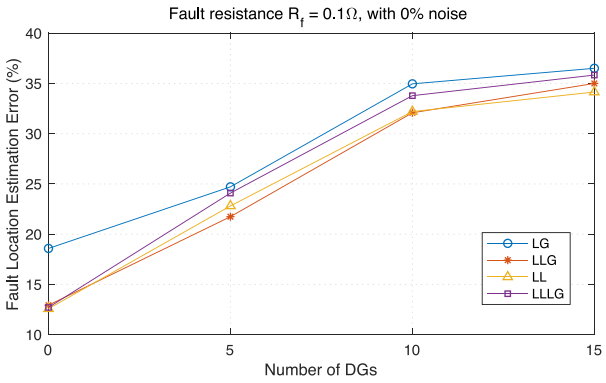

Fig. 6. FL estimation errors of four types of faults in presence of 0, 5, 10, and 15 DGs.

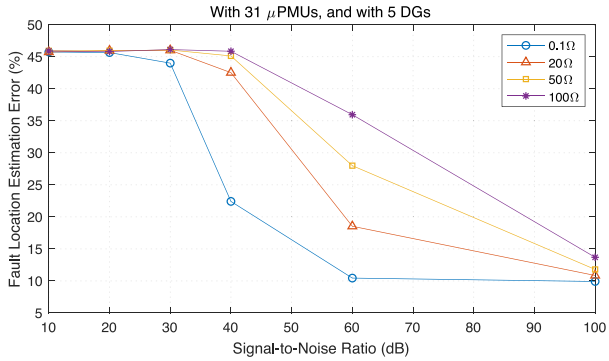

Fig. 7. FL estimation errors for the cases of different signal-to-noise ratios and with fault resistance $R_f = 0.1$, 20, 50, and 100 Ω.

the impacts of the noises at measurement units, each measured phasor value is mixed with a complex Gaussian noise $N(0, \sigma)$ whose real and imaginary parts are randomly generated with zero mean and standard derivation σ. The measurement noise levels are evaluated using the signal-to-noise ratio (SNR) of the measured voltage. In order to access the performance of the proposed method under different Gaussian noise level, the proposed method is tested under the 31-monitor placement with noise standard derivation σ varying among 0.001%, 0.1%, 1%, 3.16%, 10% and 31.62%, which correspond to the SNR of 100 dB, 60 dB, 40 dB, 30 dB, 20 dB and 10 dB, respectively. This measurement noise assessment is carried out with four different fault resistances, as presented in Fig. 7. As shown, the FL estimation error for $R_f = 0.1\ \Omega$ does not change notably when the SNR varies among $40-100$ dB. However, the FL error is elevated to 44% when the SNR decreases to 30 dB. Then the FL error reaches around 45%, as the SNR degrades to 20 dB or even lower. Considering that the accuracy class of monitor measurement usually varies from 0.1% to 0.5%, the performance of the proposed method for the low-resistance faults is within a satisfactory range under typical noise condition [28]. On the other hand, the proposed method can generate better results by utilizing the μPMUs with higher de-noising ability.

D. Impacts of Fault Resistance

Fig. 7 also evinces that higher fault resistances lead to the increasing FL estimation errors in presence of noise. Note that with the slight measurement noise (SNR = 100 dB), the FL accuracies for both low and high fault resistances are satisfactory and do not vary significantly. When the SNR continues to decrease, the FL accuracy suffers a worse degradation in the cases of high fault resistance cases. However, the FL errors for high-resistance faults are still acceptable when SNR degrades to 60 dB, which implies that the performance of the proposed method is not significantly affected by the fault resistance values under proper noise levels.

E. Impacts of Sampling Rate

The sampling rate may also affect FL accuracy. To investigate the impact of different sampling rate, the voltage measurements are derived in three sampling frequencies 1×10^4 Hz, 5×10^3 Hz and 1×10^3 Hz, which correspond to 167 samples/cycle, 83 samples/cycle and 17 samples/cycle, respectively. Fig. 8 presents the FL estimation errors at each line for LG fault. As depicted, the errors vary slightly at the majority of lines, while these errors differ notably at around 20 lines. However, the average FL error is 10.92% under the sampling frequency of 1×10^4 Hz, 11.46% under 5×10^3 Hz, and 11.91% under 1×10^3 Hz. Therefore, decreasing the sampling rate does not deteriorate the accuracy in the proposed method greatly.

F. Impacts of Synchronization Error

Synchronization errors between the μPMUs can result in the phase difference in the measured voltages and thus produce FL

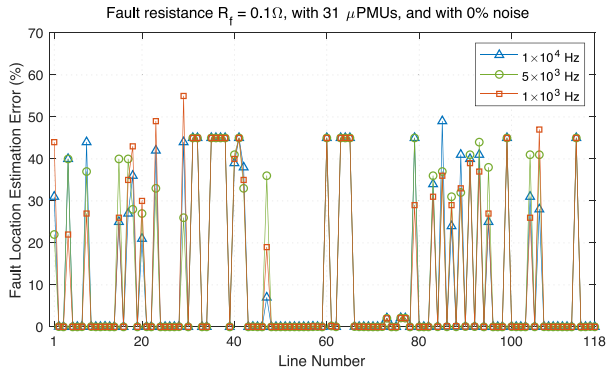

Fig. 8. FL estimation errors for the cases of single-line-to-ground fault (LG) at each line under three sampling frequencies.

TABLE II
AVERAGE AND VARIANCE OF PERCENTAGE ERRORS (%) OF FL ESTIMATION UNDER DIFFERENT LEVELS OF TOTAL VECTOR ERROR AND IMPEDANCE ERROR WITH 31 μPMUS, 5 DGS AND $R_f = 0.1\ \Omega$

Index	Without error	Total vector error (%)				Impedance error (%)			
		0.1	1	5	10	0.1	1	5	10
Avg.	9.58	14.51	33.56	40.29	44.71	10.13	14.32	29.67	36.67
Var.	4.68	5.40	8.10	7.87	7.91	4.78	5.33	7.69	7.89

errors. The difference between the theoretical voltage and the value obtained from the μPMU can be represented in the total vector error (TVE)[29]. Similarly, a Gaussian noise $N(0, \sigma_p)$ with phase standard derivation σ_p is generated and added into the phase angle of each measured voltage. As shown in Table II, the performance of the proposed method is assessed with the TVE of 0.1%, 1%, 5%, 10%, which corresponds to the phase difference of 0.057°, 0.57°, 2.80° and 5.46°. Compared with the case without synchronization error, the FL performance is degraded but remains sufficient until the TVE rises to 1%. The FL accuracy is further degraded as the TVE continues to increase. Note that the μPMU compliance verification usually requires the maximum TVE to be 1% [29]. Therefore, the acceptable performance of the proposed method is ensured in practice.

G. Impacts of Line Impedance Error

Line impedance uncertainty can affect the FL accuracy by corrupting the value of the MLIS set that is utilized to derive the exact FL. To assess such impacts, complex Gaussian noises $N(0, \sigma_l)$ with standard deviation σ_l are mixed with the series impedance and shunt admittance of each line. The FL performances for impedance error $\sigma_l = 0.1\%, 1\%, 5\%, 10\%$ are tested and also summarized in Table II. As shown, the FL can be accurately estimated until the impedance error rises to 5%. Besides, from the comparison between the cases of the TVE and the line impedance error, it can be seen that the proposed method is less sensitive to line impedance error than the synchronization error.

TABLE III
AVERAGE AND VARIANCE OF PERCENTAGE ERRORS (%) OF FL ESTIMATION FOR LG FAULT IN TWO GROUNDING MODES AND UNDER DIFFERENT NOISE LEVELS WITH 31 μPMUS, 5 DGS AND $R_f = 0.1\ \Omega$

Grounding	Index	Without noise	Signal-to-noise ratio (dB)		
			60	40	30
Solid grounding	Avg.	10.92	12.15	20.93	40.59
	Var.	4.86	5.10	6.83	7.62
Low-current grounding	Avg.	10.39	12.23	23.07	43.64
	Var.	4.99	5.27	6.96	7.53

TABLE IV
AVERAGE AND VARIANCE OF PERCENTAGE ERRORS (%) OF FL ESTIMATION FROM TWO TYPES OF METHODS WITH 16 μPMUS AND $R_f = 0.1\ \Omega$

Tested cases	Index	Type-I method	Type-II method
With 5 DGs	Avg.	0.5097	36.29
	Var.	0.0662	8.21
Without DGs	Avg.	0.5097	23.11
	Var.	0.0663	7.96

H. Impacts of Different Grounding Mode

Using low-current grounding mode attenuates the fault characteristics of the LG faults [30]. The results of the proposed method for the LG fault with a neutral grounding resistance of 0 Ω (solid grounding) and 25 Ω (low-current grounding) are presented in Table III. Compared with the solid grounding mode, the average FL error in low-current grounding mode increases slightly with the decreasing SNR, while the error variance does not vary notably. Consequently, the proposed method shows good performance even in a low-current grounded system.

I. Effectiveness in Different Scenarios

In Table I, among all tested combinations of monitor allocations as well as fault resistances, the availability of DGs, the maximum difference of the estimation errors between four fault types do not surpass 10%, which reveals that the proposed method can accurately locate the fault position for all types of faults.

Table IV presents the average and variance of estimation errors yielded by two types of FL methods introduced in Section III. The test is executed under the 16-monitor placement and noise-free measurements. Comparison between the two types of methods shows that the type-I method can estimate the fault location more accurately, with around 0.5% errors. As discussed in Section IV, the type-I method works in the cases where the fault current is fully derivable, and thus sufficient information is provided for estimating FL with negligible errors. On the other hand, considering the degradation of the given fault-current information, the type-II method still generates precise fault-location estimation with acceptable errors. Therefore, the proposed methods show satisfactory utility and applicability in practice.

TABLE V
AVERAGE OF PERCENTAGE ERRORS (%) OF FL ESTIMATION FOR THE SCHEME PROPOSED IN THIS PAPER AND IN [11] (MAJIDI'S SCHEME) UNDER 1% NOISE

Tested cases	Tested scheme	No. of PMUs	Fault types			
			LG	LLG	LL	LLLG
$R_f = 0.1\Omega$, with 5 DGs	Proposed	31	20.93	21.31	27.01	21.67
	Majidi's	34	36.10	40.11	41.10	42.01
$R_f = 20\Omega$, with 5 DGs	Proposed	31	36.95	42.93	44.84	44.71
	Majidi's	34	36.11	44.11	44.75	42.10
$R_f = 0.1\Omega$, with 10 DGs	Proposed	18	39.73	39.76	42.44	43.17
	Majidi's	25	45.93	47.46	48.10	47.33
$R_f = 0.1\Omega$, with 15 DGs	Proposed	26	43.07	42.27	43.35	43.05
	Majidi's	35	46.61	48.73	48.74	48.67

J. Discussion and Comparison

To investigate the advantage of the proposed method over the other FL methods, a comparison between the proposed method and the method introduced in [11] (Majidi's method) is carried out. Both of the proposed method and Majidi's method utilize the impedance data and sparse voltage measurements to estimate the FL in the distribution system with DG units. In Majidi's method, the monitored buses are determined by a generalized monitor allocation algorithm to satisfy the requirement of the FL scheme.

As presented in Table V, the direct comparison between the proposed method and Majidi's method is carried out in four cases. To simulate the real cases, the noises of 1% standard deviation are added into the measured voltages that are provided for both methods. For the proposed method, the number of monitors is 31 (TS3), 18 (TS4) and 26 (TS5) for the cases of 5 DGs, 10 DGs and 15 DGs, whereas 34, 25 and 35 monitors are adopted for Majidi's method, due to the requirement of Majidi's method that all DG-connected buses should be monitored.

In the implementation of Majidi's method, the shunt admittances for each line are removed because they are not taken into consideration. Instead of the precise FL along the line, Majidi's method locates the faulty buses. Therefore, Majidi's method is tested for the cases of 10% and 90% FL since the fault points are close to a bus in these cases. It can be seen from Table V that both methods suffer degradation with the increasing number of DGs. However, the proposed method produces less error in all fault types with 0.1 Ω fault resistance. Besides, the difference between FL errors from the two tested methods is not significant when the fault resistance increases to 20 Ω. In these cases, the proposed method is still superior since it requires less number of μPMUs.

The major difference between the proposed method and Majidi's method is the FL representation. The proposed method can obtain the per-unit fault position at the line, whereas Majidi's method determines the bus that is the closest to the fault point. Therefore Majidi's method generates larger errors by intrinsic. On the other hand, in Majidi's monitor placement method, the factors such as the minimum number of monitor and the cost of allocation at each bus are not considered. As a result, the monitor placement obtained by Majidi's method may not be the most cost-efficient solution.

Other impedance-based methods in [6], [31] use the voltages and currents measured at the substation and the DG-connected buses. Although this method requires less number of monitors, the measurement of fault current contribution at the substation and DG buses may produce considerable errors due to the CT saturation.

Reference [7] utilizes the sparse voltage measurement to identify the fault bus by the compressive sensing technique. In [9], the fault area is determined from the information provided by the fault indicators. However, in these methods, the impact of DGs is not investigated, and the precise FL along the faulty line is not studied.

The method in [10] locates the fault by using the voltage information from the sub-laterals. Compared with the proposed method, the method in [10] does not apply to the ungrounded fault, such as the line-to-line fault (LL).

The traveling-based methods such as [12]–[14] make use of the transient fault characteristics to estimate the FL. Therefore, these methods usually require monitors with high sampling rates. However, the aforementioned case studies show that the proposed method is not sensitive to the impact of the sampling rate, which indicates the superiority of the proposed method under the conditions of low sampling rates.

These discussions above lead to the conclusion that the proposed method gives satisfactory improvements in FL accuracy and outperforms other methods in some aspects.

Finally, it is noted that the protection devices are deactivated in the simulated system. In practice, these devices isolate the fault within a particular area, and the number of candidate faulty lines is therefore reduced, which will enhance the performance of the proposed method. Also, with the massively parallel computing technique emerging as a new approach to handle the highly computational challenges [32], the time consumption of the proposed method can be further improved and will not become a significant problem.

VI. CONCLUSION

In this paper, a sparse voltage measurement-based FL scheme is developed for distribution networks with DG. Several candidates faulted lines are selected by applying the linear least square method. Depending on the fault current solvability, two types of exact FL approaches are used to determine the faulty line as well as the precise FL. Generally, the introduced FL method is compatible with the intrinsic features of the distribution networks and immune to the impacts of DGs. Moreover, a monitor allocation method is developed, aiming to optimize the cost-efficiency at different FL accuracy requirement. Finally, the effectiveness of the proposed methods is validated on the simulated IEEE 123-node test feeder.

It should be noted that, with the increasing penetration of DGs, the assumption that the DGs be distributed at nonadjacent buses may no longer hold. Further studies will extend the proposed approaches for compatibility with this case. Besides, the impact of fast tripping will also be considered in future research.

APPENDIX A
DERIVATION OF EQUATION (11)–(13)

For a line segment of per-unit length l, the parameters $[A]$, $[B]$, $[C]$ and $[D]$ are defined as functions of l:

$$[A(l)] = [D(l)] = [I] + 0.5 \cdot l^2 \cdot [z] \cdot [y] \tag{40}$$

$$[B(l)] = l \cdot [z] \tag{41}$$

$$[C(l)] = l \cdot [y] + 0.25 \cdot l^3 \cdot [y] \cdot [z] \cdot [y] \tag{42}$$

where $[z]$ and $[y]$ stands for the line series impedance matrix and shunt admittance matrix.

Defining G_1, G_2, X_1, X_2, Q_1 and Q_2 as follows:

$$\begin{aligned} G_1 = {} & C(m) + A(m') \cdot B(m')^{-1} \cdot A(m) \\ & - (A(m) + A(m') \cdot B(m')^{-1} \\ & \cdot B(m)) \cdot A(1) \cdot B(1)^{-1} \end{aligned} \tag{43}$$

$$\begin{aligned} G_2 = {} & C(m') - A(m') \cdot B(m')^{-1} \cdot A(m') \\ & + (A(m) + A(m') \cdot B(m')^{-1} \cdot B(m)) \\ & \cdot (-C(1) + A(1) \cdot B(1)^{-1} \cdot A(1)) \end{aligned} \tag{44}$$

$$X_1 = A(m) - B(m) \cdot A(1) \cdot B(1)^{-1} - B(m') \cdot B(1)^{-1} \tag{45}$$

$$\begin{aligned} X_2 = {} & B(m) \cdot (-C(1) + A(1) \cdot B(1)^{-1} \cdot A(1)) - A(m') \\ & + B(m') \cdot B(1)^{-1} \cdot A(1) \end{aligned} \tag{46}$$

$$Q_1 = A(m) + A(m') \cdot B(m')^{-1} \cdot B(m) \tag{47}$$

$$\begin{aligned} Q_2 = {} & -(X_1 \cdot Z_{ij} + X_2 \cdot Z_{jj} - B(m'))^{-1} \\ & \cdot (X_1 \cdot Z_{ii} + X_2 \cdot Z_{ij} + B(m)) \end{aligned} \tag{48}$$

Combining (4), (6) and (9) as well as the coefficients predefined in (43)–(47):

$$I_{\mathrm{f}j} = Q_2 \cdot I_{\mathrm{f}i} \tag{49}$$

$$\begin{aligned} I_f = {} & (G_1 \cdot Z_{ii} + G_2 \cdot Z_{ij} + Q_1) \cdot I_{\mathrm{f}i} \\ & + (G_1 \cdot Z_{ij} + G_2 \cdot Z_{jj}) \cdot I_{\mathrm{f}j} \end{aligned} \tag{50}$$

$$\Delta U_F^{(\mathrm{fp})} = H_1 \cdot I_{\mathrm{f}i} + H_2 \cdot I_{\mathrm{f}j} \tag{51}$$

where H_1 and H_2 are defined as follows:

$$\begin{aligned} H_1 = {} & (A(m) - B(m) \cdot A(1) \cdot B^{-1}) \cdot Z_{ii} \\ & + B(m) \cdot (-C(1) + A(1) \cdot B^{-1} \cdot A(1)) \cdot Z_{ij} + B(m) \end{aligned} \tag{52}$$

$$\begin{aligned} H_2 = {} & (A(m) - B(m) \cdot A(1) \cdot B^{-1}) \cdot Z_{ij} \\ & + B(m) \cdot (-C(1) + A(1) \cdot B(1)^{-1} \cdot A(1)) \cdot Z_{jj} \end{aligned} \tag{53}$$

By substituting (49) into (50) (51), $I_{\mathrm{f}i}$, $I_{\mathrm{f}j}$ and ΔU_F can be expressed in terms of I_f with two coefficients T_1, T_2 determined as follows:

$$\begin{aligned} T_1 = {} & ((G_1 \cdot Z_{ii} + G_2 \cdot Z_{ij} + Q_1) \\ & + (G_1 \cdot Z_{ij} + G_2 \cdot Z_{jj}) \cdot Q_2)^{-1} \end{aligned} \tag{54}$$

$$T_2 = Q_2 \cdot T_1 \tag{55}$$

The relations described in (11)–(13) are thus obtained. In addition, combining (4) and (6) results:

$$\Delta U_F^{(\mathrm{dg})} = W_1 \cdot \Delta U_i^{(\mathrm{dg})} + W_2 \cdot \Delta U_j^{(\mathrm{dg})} \tag{56}$$

where W_1, W_2 are defined as follows:

$$\begin{aligned} W_1 = {} & (A(m) \cdot B(m)^{-1} + A(m') \cdot B(m')^{-1})^{-1} \\ & \cdot (A(m) \cdot B(m)^{-1} \cdot A(m) - C(m)) \end{aligned} \tag{57}$$

$$\begin{aligned} W_2 = {} & (A(m) \cdot B(m)^{-1} + A(m') \cdot B(m')^{-1})^{-1} \\ & \cdot (A(m') \cdot B(m')^{-1} \cdot A(m') - C(m')) \end{aligned} \tag{58}$$

By substituting (10) into (56), and using T_3 to represent $(H_1 \cdot T_1 + H_2 \cdot T_2)$, equation (13) can be derived.

APPENDIX B
DERIVATION OF COEFFICIENTS FOR COMPLETE CASE

Substituting (43)–(46), (54) and (55) in (11) and (12), then eliminating I_f and expanding with (40)–(42):

$$\begin{aligned} a_2 = {} & 0.5 \cdot z \cdot y \cdot Z_{ii} \cdot I_{\mathrm{f}i} - 0.5 \cdot z \cdot y \cdot Z_{ij} \cdot I_{\mathrm{f}i} \\ & + 0.5 \cdot z \cdot y \cdot Z_{ij} \cdot I_{\mathrm{f}j} - 0.5 \cdot z \cdot y \cdot Z_{jj} \cdot I_{\mathrm{f}j} \end{aligned}$$

$$\begin{aligned} a_1 = {} & Z_{ii} \cdot I_{\mathrm{f}i} - Z_{ij} \cdot I_{\mathrm{f}i} + Z_{ij} \cdot I_{\mathrm{f}j} - Z_{jj} \cdot I_{\mathrm{f}j} \\ & + 0.5 \cdot z \cdot y \cdot Z_{ij} \cdot I_{\mathrm{f}i} + 0.5 \cdot z \cdot y \cdot Z_{jj} \cdot I_{\mathrm{f}j} \\ & + Z_{ij} \cdot I_{\mathrm{f}i} + \cdot Z_{jj} \cdot I_{\mathrm{f}j} - Z_{ii} \cdot I_{\mathrm{f}i} - Z_{ij} \cdot I_{\mathrm{f}j} \\ & - 0.25 \cdot z \cdot y \cdot z \cdot y \cdot Z_{ij} \cdot I_{\mathrm{f}i} \\ & - 0.25 \cdot z \cdot y \cdot z \cdot y \cdot Z_{jj} \cdot I_{\mathrm{f}j} \\ & - 0.5 \cdot z \cdot y \cdot Z_{ij} \cdot I_{\mathrm{f}i} - 0.5 \cdot z \cdot y \cdot Z_{jj} \cdot I_{\mathrm{f}j} \\ & + 0.5 \cdot z^2 \cdot y \cdot z^{-1} \cdot Z_{ij} \cdot I_{\mathrm{f}i} + 0.5 \cdot z^2 \cdot y \cdot z^{-1} \cdot Z_{jj} \cdot I_{\mathrm{f}j} \\ & - 0.5 \cdot z^2 \cdot y \cdot z^{-1} \cdot Z_{ii} \cdot I_{\mathrm{f}i} - 0.5 \cdot z^2 \cdot y \cdot z^{-1} \cdot Z_{ij} \cdot I_{\mathrm{f}j} \\ & + 0.25 \cdot z^2 \cdot y^2 \cdot Z_{ij} \cdot I_{\mathrm{f}i} + 0.25 \cdot z^2 \cdot y^2 \cdot Z_{jj} \cdot I_{\mathrm{f}j} \\ & + z \cdot I_{\mathrm{f}i} + z \cdot I_{\mathrm{f}j} \end{aligned}$$

$$a_0 = -z \cdot I_{\mathrm{f}j}$$

REFERENCES

[1] M. Saha, J. Izykowski, and E. Rosolowski, *Fault Location on Power Networks*. Berlin, Germany: Springer, 2009.

[2] T. N. Boutsika and S. A. Papathanassiou, "Short-circuit calculations in networks with distributed generation," *Elect. Power Syst. Res.*, vol. 78, no. 7, pp. 1181–1191, Jul. 2008.

[3] M. E. Baran and I. El-Markaby, "Fault analysis on distribution feeders with distributed generators," *IEEE Trans. Power Syst.*, vol. 20, no. 4, pp. 1757–1764, Nov. 2005.

[4] T. H. M. EL-Fouly and C. Abbey, "On the compatibility of fault location approaches and distributed generation," in *Proc. CIGRE/IEEE PES Joint Symp. Integr. Wide-Scale Renew. Resour. Power Del. Syst.*, Jul. 2009, pp. 1–5.
[5] Y. Liao, "A novel method for locating faults on distribution systems," *Elect. Power Syst. Res.*, vol. 117, pp. 21–26, Dec. 2014.
[6] S. F. Alwash, V. K. Ramachandaramurthy, and N. Mithulananthan, "Fault-location scheme for power distribution system with distributed generation," *IEEE Trans. Power Del.*, vol. 30, no. 3, pp. 1187–1195, Jun. 2015.
[7] M. Majidi, A. Arabali, and M. Etezadi-Amoli, "Fault location in distribution networks by compressive sensing," *IEEE Trans. Power Del.*, vol. 30, no. 4, pp. 1761–1769, Aug. 2015.
[8] W. Fan and Y. Liao, "Fault identification and location for distribution network with distributed generations," *Int. J. Emerg. Elect. Power Syst.*, vol. 19, no. 3, 2018, Art. no. 20180048.
[9] I. Dzafic, R. A. Jabr, S. Henselmeyer, and T. Donlagic, "Fault location in distribution networks through graph marking," *IEEE Trans. Smart Grid*, vol. 9, no. 2, pp. 1345–1353, Mar. 2018.
[10] S. Zhang, S. Lin, Z. He, and W.-J. Lee, "Ground fault location in radial distribution networks involving distributed voltage measurement," *IET Gener., Transmiss. Distrib.*, vol. 12, no. 4, pp. 987–996, Feb. 2018.
[11] M. Majidi and M. Etezadi-Amoli, "A new fault location technique in smart distribution networks using synchronized/nonsynchronized measurements," *IEEE Trans. Power Del.*, vol. 33, no. 3, pp. 1358–1368, Jun. 2018.
[12] A. Esmaeilian and M. Kezunovic, "Fault location using sparse synchrophasor measurement of electromechanical-wave oscillations," *IEEE Trans. Power Del.*, vol. 31, no. 4, pp. 1787–1796, Aug. 2016.
[13] S. Shi, B. Zhu, A. Lei, and X. Dong, "Fault location for radial distribution network via topology and reclosure-generating traveling waves," *IEEE Trans. Smart Grid*, vol. 10, no. 6, pp. 6404–6413, Nov. 2019, doi: 10.1109/TSG.2019.2904210.
[14] K. Jia, T. Bi, Z. Ren, D. W. P. Thomas, and M. Sumner, "High frequency impedance based fault location in distribution system with DGS," *IEEE Trans. Smart Grid*, vol. 9, no. 2, pp. 807–816, Mar. 2018.
[15] M. Majidi, M. Etezadi-Amoli, and M. Sami Fadali, "A novel method for single and simultaneous fault location in distribution networks," *IEEE Trans. Power Syst.*, vol. 30, no. 6, pp. 3368–3376, Nov. 2015.
[16] M. Shafiullah, M. Abido, and T. Abdel-Fattah, "Distribution grids fault location employing ST based optimized machine learning approach," *Energies*, vol. 11, no. 9, Sep. 2018, Art. no. 2328.
[17] E. A. Reche, J. V. de Sousa, D. V. Coury, and R. A. S. Fernandes, "Data mining-based method to reduce multiple estimation for fault location in radial distribution systems," *IEEE Trans. Smart Grid*, vol. 10, no. 4, pp. 3612–3619, Jul. 2019, doi: 10.1109/TSG.2018.2832840.
[18] W. H. Kersting, *Distribution System Modeling and Analysis, Fourth Edition*. Boca Raton, FL, USA: CRC Press, Aug. 2017.
[19] E. B. Makram, M. A. Bou-Rabee, and A. A. Girgis, "Three-phase modeling of unbalanced distribution systems during open conductors and/or shunt fault conditions using the bus impedance matrix," *Elect. Power Syst. Res.*, vol. 13, no. 3, pp. 173–183, 1987.
[20] P. T. Manditereza and R. Bansal, "Renewable distributed generation: The hidden challenges: A review from the protection perspective," *Renew. Sustain. Energy Rev.*, vol. 58, pp. 1457–1465, 2016.
[21] G. Xiangqian, K. Hongwen, and C. Hongxing, "The least-square method in complex number domain," *Prog. Natural Sci.*, vol. 16, no. 3, pp. 307–312, 2006.
[22] J. Lagarias, J. Reeds, M. Wright, and P. Wright, "Convergence properties of the Nelder–Mead simplex method in low dimensions," *SIAM J. Optim.*, vol. 9, no. 1, pp. 112–147, 1998.
[23] J. D'Errico, "fminsearchbnd, fminsearchcon," Feb. 2012. [Online]. Available: http://www.mathworks.com/matlabcentral/fileexchange/8277-fminsearchbnd
[24] Y. Liao, "Fault location observability analysis and optimal meter placement based on voltage measurements," *Elect. Power Syst. Res.*, vol. 79, no. 7, pp. 1062–1068, Jul. 2009.
[25] M. T. M. Emmerich and A. H. Deutz, "A tutorial on multiobjective optimization: Fundamentals and evolutionary methods," *Natural Comput.*, vol. 17, no. 3, pp. 585–609, May 2018.
[26] K. Deb, S. Agrawal, A. Pratap, and T. Meyarivan, "A fast elitist non-dominated sorting genetic algorithm for multi-objective optimization: NSGA-II," in *Parallel Problem Solving from Nature PPSN VI*. Berlin, Germany: Springer, Sep. 2000, pp. 849–858.
[27] *IEEE Guide for Determining Fault Location on AC Transmission and Distribution Lines*, IEEE Std C37.114-2014 (Revision of IEEE Std C37.114-2004), pp. 1–76, Jan. 2015.
[28] T. Solvang, L. Aleixo, and H. Seljeseth, "Power quality measurement capabilities of "smart" energy meters," *Renew. Energy Power Qual. J.*, vol. 1, no. 08, pp. 695–699, Apr. 2010.
[29] *IEEE/IEC International Standard—Measuring Relays and Protection Equipment - Part 118-1: Synchrophasor for Power Systems—Measurements*, IEC/IEEE 60255-118-1:2018, pp. 1–78, Dec. 2018.
[30] M. Bollen, "Voltage sags in three-phase systems," *IEEE Power Eng. Rev.*, vol. 21, no. 9, pp. 8–15, Sep. 2001.
[31] R. Dashti, M. Ghasemi, and M. Daisy, "Fault location in power distribution network with presence of distributed generation resources using impedance based method and applying π line model," *Energy*, vol. 159, pp. 344–360, Sep. 2018.
[32] C. Dobre and F. Xhafa, "Parallel programming paradigms and frameworks in big data era," *Int. J. Parallel Program.*, vol. 42, no. 5, pp. 710–738, Oct. 2014.

Haotian Sun received the B.S. degree in electrical engineering from Xi'an Jiaotong University, Xi'an, China, in 2017, where he is currently working toward the M.S. degree in the Department of Electrical Engineering.

His research interests include power quality improvement and fault location in distribution system.

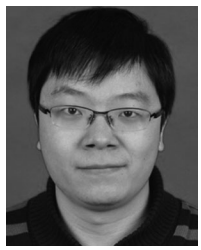

Hao Yi (S'10–M'14) received the M.S. and Ph.D. degrees in electrical engineering from Xi'an Jiaotong University (XJTU), Xi'an, China, in 2010 and 2013, respectively.

Since 2013, he has been a member of the School of Electrical Engineering, XJTU. His current research interests include modeling and control of high-power converters, control and power management of microgrids, and power quality improvement.

Fang Zhuo (M'00) was born in Shanghai, China, in 1962. He received the B.S. degree in automatic control and the M.S. and Ph.D. degrees in automation and electrical engineering all from Xi'an Jiaotong University (XJTU), Xi'an, China, in 1984, 1989, and 2001, respectively.

He was an Associate Professor with XJTU in 1996 and a Full Professor in power electronics and drives in 2004. He was a Supervisor of Ph.D. students. He is also the Power Quality Professional Chairman of the Power Supply Society in China. His research interests include power electronics, power quality, active power filter, reactive power compensation, and inverters for distributed power generation. He is a member of the China Electro Technical Society, Automation Society, and Power Supply Society.

Xiaotong Du was born in Hebei, China. She received the B.S. and M.S. degrees in electrical engineering from Xi'an Jiaotong University, Shaanxi, China in 2016 and 2019, respectively. She is currently working toward the Ph.D. degree in the École polytechnique fédérale de Lausanne.

Her current research interests include power electronic transformer designing.

Guangyu Yang was born in Anhui, China. He received the B.S. degree in electrical engineering from Hefei University of Technology, Hefei, China, in 2017.

His current research interests include power quality improvement and micro-grid management.